Chapter 7*

Balanced Electronic Detection of Displacement in Nanoelectromechanical Systems

We describe a broadband radio frequency balanced bridge technique for electronic detection of displacement in nanoelectromechanical systems (NEMS). With its two-port actuation-detection configuration, this approach generates a background-nulled electromotive force in a dc magnetic field that is proportional to the displacement of the NEMS resonator. We demonstrate the effectiveness of the technique by detecting small impedance changes originating from NEMS electromechanical resonances that are accompanied by large static background impedances at very high frequencies. This technique allows the study of important experimental systems such as doped semiconductor NEMS and may provide benefits to other high frequency displacement transduction circuits.

© *2002 American Institute of Physics.* [DOI: 10.1063/1.1507833]

* This section has been published as: K. K. L. Ekinci, Y. T. Yang, X. M. H. Huang, and M. L. Roukes, *Appl. Phys. Lett.* **78** 162 (2002).

7.1 Introduction

The recent efforts to scale microelectromechanical systems (MEMS) down to the submicron domain[1] have opened up an active research field. The resulting nanoelectromechanical systems (NEMS) with fundamental mechanical resonance frequencies reaching into the microwave bands are suitable for a number of important technological applications. Experimentally, they offer potential for accessing interesting phonon mediated processes and the quantum behavior of mesoscopic mechanical systems.

Among the most needed elements for developing NEMS based technologies—as well as for accessing interesting experimental regimes—are broadband, on-chip transduction methods sensitive to subnanometer displacements. While displacement detection at the scale of MEMS has been successfully realized using magnetic,[2] electrostatic[3,4] and piezoresistive[5] transducers through electronic coupling, most of these techniques become insensitive at the submicron scales.

7.2 Circuit Schemes and Measurement Results

An on-chip displacement transduction scheme that scales well into the NEMS domain and offers direct electronic coupling to the NEMS displacement is magnetomotive detection.[6,7] Magnetomotive reflection measurements as shown schematically[8] in figure 7.1(a) have been used extensively.[6,7,9] Here, the NEMS resonator is modeled as a parallel *RLC* network with a mechanical impedance, $Z_m(\omega)$, a two-terminal dc coupling resistance, R_e, and mechanical resonance frequency, ω_0. When

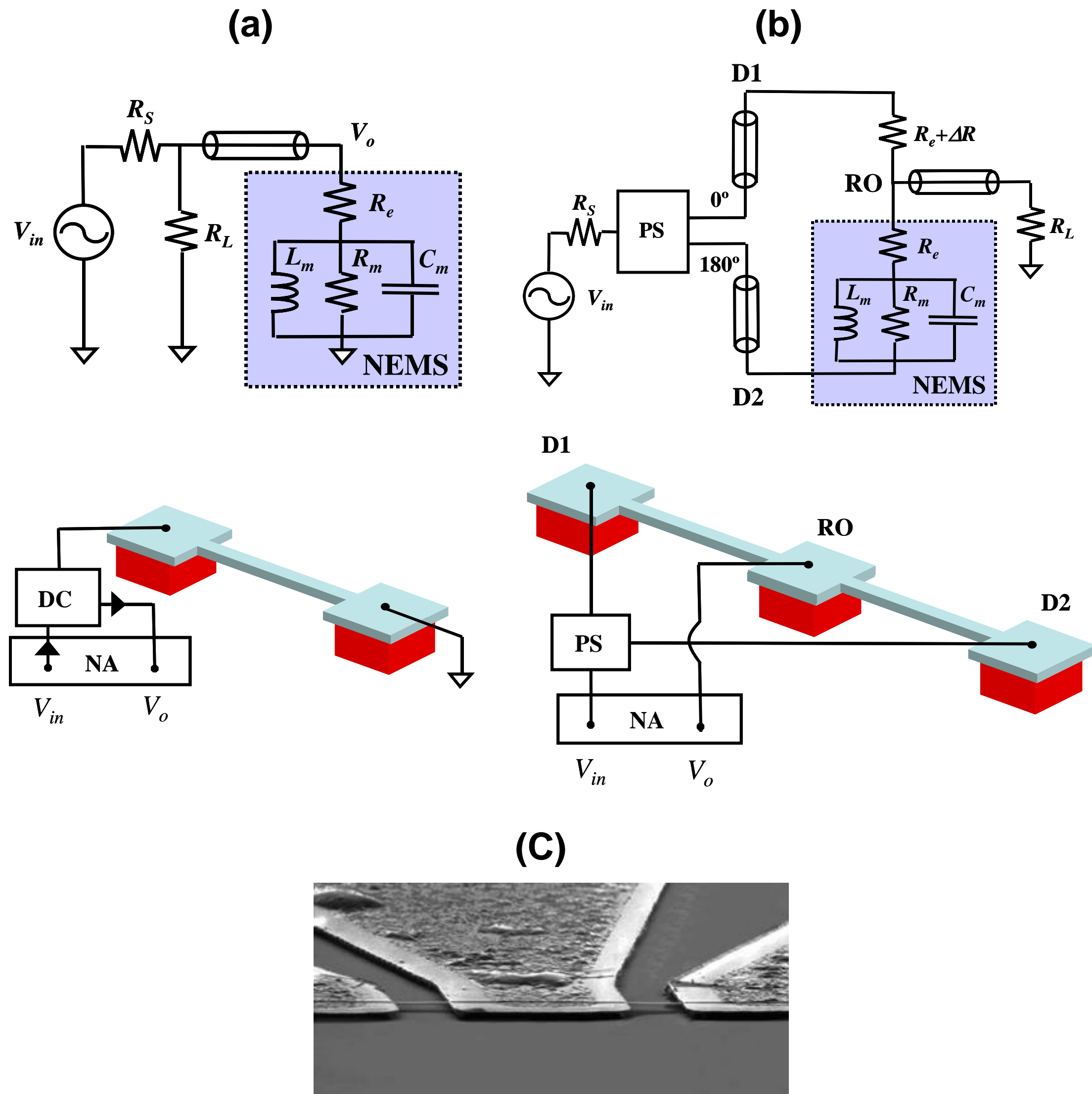

Figure 7.1. Schematic diagrams for the magnetomotive reflection measurement and bridge measurement (a) Schematic diagram for the magnetomotive reflection mesurement. In both reflection and bridges measurements, a network analyzer (NA) supplies the drive voltage, V_{in}. In reflection measurement, a directional coupler (DC) is implemented to access the reflected signal from the device. **(b) Schematic diagram for the magnetomotive bridge measurement.** V_{in} is split into two out-of-phase components by a power splitter (PS) before it is applied to ports D1 and D2. (c) Scanning electron micrograph of a representative bridge device, from an epitaxially grown wafer with 50 nm thick n^+ GaAs and 100 nmGaAs structure layer on top. The doubly clamped beams with dimensions of 8 μm(L) × 150 nm(w) × 500 nm(t) at the two arms of the bridge have in plane fundamental flexural mechanical resonances at ~35 MHz. D1, D2, and RO ports on the device are as shown.

driven at ω by a source with impedance R_s, the voltage on the load, R_L, can be approximated as

$$V_0(\omega) = V_{in}(\omega)\frac{R_e + Z_m(\omega)}{R_L + (R_e + Z_m(\omega))} \cong V_{in}(\omega)\frac{R_e + Z_m(\omega)}{R_L + R_e}. \tag{7.1}$$

Here, $R_L = R_S = 50\Omega$. We have made the approximation that $R_e >> |Z_m(\omega)|$, as is the case in most experimental systems. Apparently, the measured electromotive force (EMF) due to the NEMS displacement proportional to $|Z_m(\omega)|$ is embedded in a background close to the drive voltage amplitude, $|V_0| \sim |V_{in}| - 20\log R_e/(R_L + R_e)$ dB.[10] This facilitates the definition of a useful parameter at $\omega = \omega_0$, the detection *efficiency*, *S/B*, as the ratio of the signal voltage to the background. For the reflective, one-port magnetomotive measurement of figure 7.1(a), $S/B = Z_m(\omega_0)/R_e = R_m/R_e$, indicating some shortcomings. First, detection of the EMF becomes extremely challenging, when $R_e << R_m$, i.e., in unmetallized NEMS devices or metallized high frequency NEMS (small R_m). Second, the voltage background prohibits the use of the full dynamic range of the detection electronics. In addition to the balanced bridge detection here, we describe two-port schem to improve the detection efficiency, i.e., *S/B* ratio.[11]

The balanced circuit shown in figure 7.1(b) with a NEMS resonator on one side of the bridge and a matching resistor of resistance, $R = R_e + \Delta R$ on the other side, is designed to improve *S/B*. The voltage, $V_0(\omega)$ at the readout (RO) port is nulled for $\omega \neq \omega_0$, by applying two 180° out of phase voltages to the Drive 1 (D1) and Drive 2 (D2) ports in the circuit. We have found that the circuit can be balanced with exquisite sensitivity, by fabricating two identical doubly clamped beam resonators on either side of

the balance point (RO), instead of a resonator and a matching resistor, as shown in figure 7.1(c). In such devices, we almost always obtained two well-separated mechanical resonances, one from each beam resonator, with $|\omega_2 - \omega_1| >> \omega_1 / Q$ where ω_i and Q are the resonance frequency and the quality factor of resonance of the resonators (i=1,2) (see figure 7.3). This indicates that in the vicinity of either mechanical resonance, the system is well described by the mechanical resonator-matching resistor model of figure 7.1(b). We attribute this behavior to the high Q factors ($Q \geq 10^3$) and the extreme sensitivity of the resonance frequencies to local variations of parameters during the fabrication process.

First, to clearly assess the improvements, we compared reflection and balanced bridge measurements of the fundamental flexural resonances of doubly clamped beams patterned from n^+ (B-doped) Si as well as from n^+ (Si-doped) GaAs. Electronic detection of mechanical resonances of these types of NEMS resonators have proven to be Challenging,[12] since for these systems $R_e \geq 2k\Omega$ and $R_m \leq R_e$. Nonetheless, with the bridge technique we have detected fundamental flexural resonances in the 10 MHz< f_0 <85 MHz range for n^+ Si resonators and in the 7 MHz < f_0 <35 MHz range for n^+ GaAs beams. In all our measurements, the paradigm that $R_m << R_e$ remained true as $R_m = 10\,\Omega$ and 2 kΩ< R_e <20 kΩ. Here, we focus on our results from n^+ Si beams. These were fabricated from a B-doped Si on insulator wafer, with Si layer and buried oxide layer thicknesses of 350 and 400 nm, respectively. The doping was done at 950 °C. The dopant concentration was estimated as $N_d \approx 6x10^{19}$ cm^{-3} from the sample sheet resistance, $R_\square$=60 Ω.[13] The fabrication of the actual devices involved optical lithography, electron beam lithography, and lift-off steps followed by anisotropic electron cyclotron resonance

plasma and selective HF wet etches.[7,9,12] The electromechanical response of the bridge was measured in a magnetic field generated by a superconducting solenoid. Figure 7.2(a) shows the response of a device with dimensions 15 μm(L) × 500 nm(w) × 350 nm(t) and with $R_e = 2.14\,\mathrm{k}\Omega$, measured in the reflection (upper curves) And bridge configurations for several magnetic field strengths. The device has an in plane flexural resonance at 25.598 MHz with $Q = 3x10^4$ at $T = 20\,\mathrm{K}$. With $\Delta R \approx 10\,\Omega$ a background reduction of a factor of $R_e / \Delta R = 200$ was obtained in the bridge measurements (see analysis below). Figure 7.2(b) shows a measurement of the broadband transfer functions for both configurations for comparable drives at zero magnetic field. Notice the dynamic background reduction in the relevant frequency range.

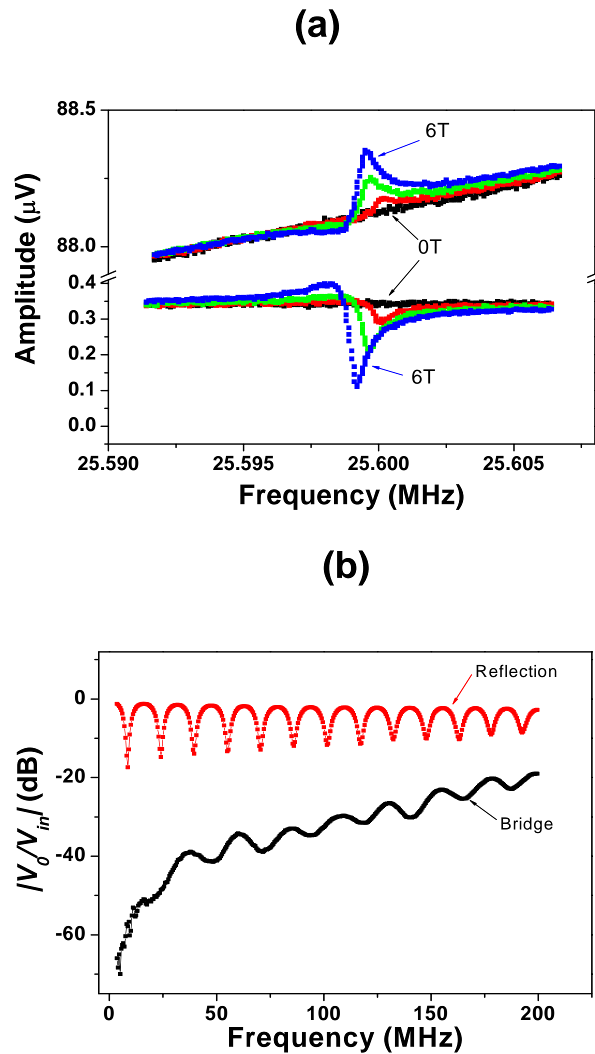

Figure 7.2 Data from a doubly clamped n$^+$ Si beam. (a) Mechanical resoanance. The mechanical resonance at 25.598 MHz with a Q~3x10^4 from a doubly clamped, n^+ Si beam is measured in reflection (upper curves) and in bridge (lower curves) configurations for magnetic field strengths of B=0,2,4,6 T. The drive voltages are equal. The background is reduced by a factor of ~200 in the bridge measurements. The phase of the resonance in the bridge measurements can be shifted 180° with respect to the drive signal (see Fig.7.1). **(b) The amplitude of the broadband transfer functions.** The broadband transfer function $H_B(\omega) = V_0(\omega)/V_{in}(\omega)$ for reflection (upper curve) and bridge (lower curve) configurations. The data indicate a background reduction of at least 20 dB and capacitive coupling between the actuation–detection ports in the bridge circuit.

Bridge measurements also provided benefits in the detection of electromechanical resonances from metallized VHF NEMS. These systems generally possess high R_e and R_m diminishes quickly as the resonance frequencies increase. Here, we present from our measurements on doubly clamped SiC beams embedded within the bridge configuration. These beams were fabricated with top metallization layers using a process described in detail.[9] For such beams with $R_e = 100\,\Omega$ and $R_m \leq 1\,\Omega$, we were able to detect mechanical flexural resonances deep into the VHF band. Figure 7.3(a) depicts a data trace of the in plane flexural mechanical resonances of two 2 μm (L) × 150 nm (w) × 80 nm (t) doubly clamped SiC beams. Two well-separated resonances are extremely prominent at 198.00 and 199.45 MHz, respectively, with Q=10^3 at T= 4.2 K. The broadband response from the same device is plotted in figure 7.3(b). A reflection measurement in the vicinity of the mechanical resonance frequency of this system would give rise to an estimated background on the order, $|V_0 / V_{in}|$=-20dB,[10] making the detection of the resonance extremely challenging.

(a)

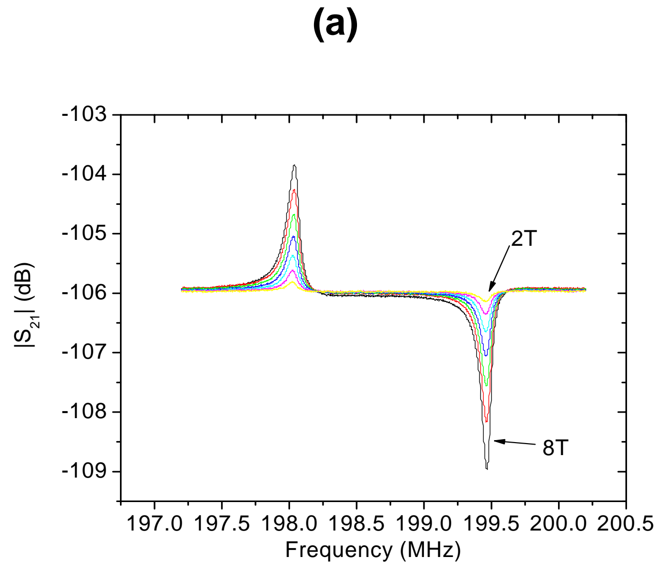

(b)

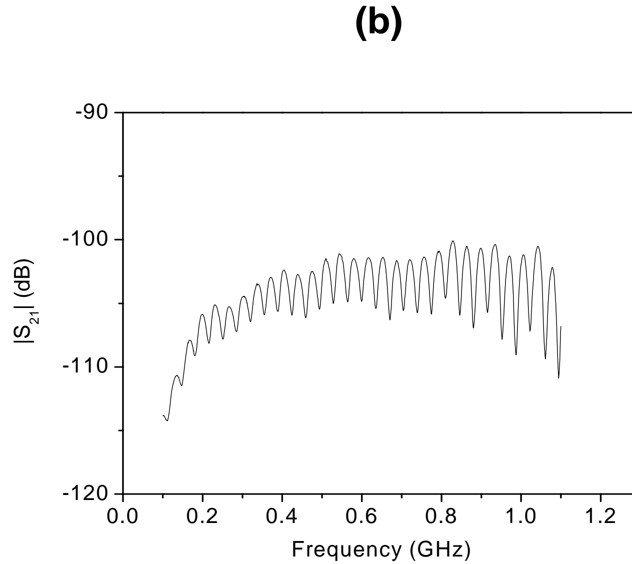

Figure 7.3. Narrow band and broadband transfer function (S_{21}) amplitudes from metallized SiC beams in bridge configuration. (a) The narrow band response. The narrowband response is measured for different magnetic field strengths of B=2, 4, 6, 8 T and shows two well-separated resonances at 198.00 and 199.45 MHz, respectively, with Q=10^3. **(b) The broadband response.** The broadband response at B=0 T shows the significant background nulling attainable in bridge measurements. We estimate that a reflection measurement on this system would produce $|V_0/V_{in}|$=20dB for $\omega \approx \omega_0$.

Figure 7.1(b) depicts our analysis of the bridge circuit. The voltage at point RO in the circuit can be determined as[14]

$$V_0(\omega) = -\frac{V_{in}(\omega)[\Delta R + Z_m(\omega)]}{(\Delta R + Z_m(\omega))(1 + R_e / R_L) + R_e(2 + R_e / R_L)} = -\frac{V_{in}(\omega)}{Z_{eq}^{'}(\omega)}[\Delta R + Z_m(\omega)], \qquad (7.2)$$

in analogy to equation (7.1). At $\omega = \omega_0, S / B = R_m / \Delta R$. Given that ΔR is small, the background is suppressed by a factor of order $R_e / \Delta R$, as compared to the one-port case as shown in figure 7.2(a). At higher frequencies, however, the circuit model becomes imprecise as is evident from the measurements of the transfer function. Capacitive coupling becomes dominant between D1, D2, and RO ports as displayed in figure 7.2(b), and this acts to reduce the overall effectiveness of the technique. With careful design of the circuit layout and the bonding pads, such problems can be minimized. Even further signal improvements can be obtained by addressing the significant impedance mismatch, $R_e \geq R_L$, between the output impedance, R_e, and the amplifier input impedance, R_L. In the measurements displayed in figure 7.2(a), this mismatch caused a signal attenuation estimated to be of order ~40 dB.

Our measurements on doped NEMS offer insight into energy dissipation mechanisms in NEMS, especially those arising from surfaces and surface adsorbates. In the frequency range investigated, 10 MHz < f_0 < 85 MHz, the measured Q factors of $2.2 \times 10^4 < Q < 8 \times 10^4$ in n^+ Si beams is a factor of 2–5 higher than those obtained from metallized beams.[15] Both metallization layers[16] and impurity dopants[3] can make an appreciable contribution to the energy dissipation. Our measurements on NEMS seem to confirm that metallization overlayers can significantly reduce Q factor. The high Q factors attained and the metal free surfaces make doped NEMS excellent tools for the

investigation of small energy dissipation changes due to surface adsorbates and defects. In fact, efficient *in situ* resistive heating in doped beams through R_e has been shown to facilitate thermal annealing[17] and desorption of surface adsorbates—yielding even higher quality factors.

7.3 Conclusion

In conclusion, we have developed a broadband, balanced radio frequency bridge technique for detection of small NEMS displacements. This technique may prove useful for other high frequency high impedance applications such as piezoresistive displacement detection. The technique, with its advantages, has enabled electronic measurements of NEMS resonances otherwise essentially unmeasurable.

References

1. M. L. Roukes Nanoelectromechanical systems face the future. *Phys. World* **14**, 25 (2001).

2. D. S. Greywall, B. Yurke, P. A. Busch, A. N. Pargellis, and R. L. Willett Evading amplifier noise in nonlinear oscillators. *Phys. Rev. Lett.* **72**, 2992 (1994).

3. R. E. Mihailovich and J. M. Parpia Low-temperature mechanical-properties of boron-doped silicon. *Phys. Rev. Lett.* **68**, 3052 (1992).

4. W. C. Tang, T. C. H. Nguyen, M. W. Judy, and R. T. Howe Electrostatic-comb drive of lateral polysilicon resonators. *Sens. Actuator* **A 21**, 328 (1990).

5. M. Tortonese, R. C. Barrett, and C. F. Quate Atomic resolution with an atomic force microscope using piezoresistive detection. *Appl. Phys. Lett.* **62**, 834 (1993).

6. A. N. Cleland and M. L. Roukes Fabrication of high frequency nanometer scale mechanical resonators from bulk Si crystals. *Appl. Phys. Lett.* **69,** 2653 (1996).

7. A. N. Cleland and M. L. Roukes External control of dissipation in a nanometer-scale radiofrequency mechanical resonator. *Sens. Actuator* **A 72**, 256 (1999).

8. To simplify, the length of the transmission line, l_t, between the NEMS and the measurement point has been set to $l_t \approx \lambda/2$ where λ is the drive wavelength. Also, the reflection coefficient, Γ, from the NEMS, defined as the ratio of the amplitudes of reflected to incident voltages, is taken as unity. Experimentally, *l* is readily adjustable and Γ closed to unity with R_e close to 100 Ω→ 1 kΩ.

9. Y. T. Yang, K. L. Ekinci, X. M. H. Huang, L. M. Schiavone, M. L. Roukes, C. A. Zorman, and M. Mehregany Monocrystalline silicon carbide nanoelectromechanical systems. *Appl. Phys. Lett.* **78**, 162 (2001).

10. When Γ≠1, $V_0 \cong \Gamma V_{in}(R_e + Z(\omega))/(R_L + R_e)$, giving a correction to the background on the order of $-20\log\Gamma$ dB.

11. See chapter 4.

12. L. Pescini, A. Tilke, R. H. Blick, H. Lorenz, J. P. Kotthaus, W. Eberhardt, and D. Kern Suspending highly doped silicon-on-insulator wires for applications in nanomechanics. *Nanotechnology* **10**, 418 (1999).

13. S. M. Sze *Physics of Semiconductor Devices* (New York, Wiley, 1981).

14. Replacing R_e with $R_e + R_S$ would produce the more general form.

15. We have qualitatively compared *Q* factors of eight metallized and 14 doped Si beams measured in different experimental runs, spanning the indicated frequency range.

16. X. Liu, E. J. Thompson, B. E. White, and R. O. Pohl Low-temperature internal friction in metal films and in plastically deformed bulk aluminum. *Phys. Rev. B* **59**, 11767 (1999).

17. K. Y. Yasumura, T. D. Stowe, E. M. Chow, T. Pfafman, T. W. Kenny, B. C. Stipe, and D. Rugar Quality factors in micron- and submicron-thick cantilevers. *J. Microelectromech. Syst.* **9**, 117 (2000).